Designing inorganic-organic nanofibers nanocomposite for Supercapacitor Applications

Omar A. Hussein[1*], T. H. Mubarak[2], Isam M. Ibrahim [3]

Abstract

This article reports to the method for fabrication of Polypyrrole nanofibers (PPy-NFs) and Co0.2Zn0.6Mn0.2Fe2O4 via chemical oxidative polymerization and co-precipitation. In addition to treatment of product ferrite in hydrothermal autoclave reactors. Later, the nanofibers are ornament with spherical ferrite nanoparticles to gain the PP-NFs nanocomposite as demonstrated in the FESEM images. The single-phase formation of Co0.2Zn0.6Mn0.2Fe2O4 and its crystal system were determined using X-ray diffraction measurements. XRD showed the amorphous nature of the PPy-NFs polymer. The electrochemical performances of the samples are studied by using cyclic voltammetry (CV), galvanostatic charge–discharge analysis (GCD) and electrochemical impedance spectroscopy (EIS) analysis. Specific capacitances of PPy-NFs and ferrite nanoparticles are 305 and 230.01 F/g, respectively. Whereas, PPy-NFs nanocomposite are equal 370.39 F/g. This means, PPy-NFs nanocomposite preparing method had showed as an applicable process which develop the redox performance of the composite material significantly exceeding of its constituents.

KeyWords: Polypyrrole nanofibers, Conducting polymer, cyclic voltammetry, co-precipitation method.
DOI Number:10.14704/nq.2022.20.1. NQ22560 **NeuroQuantology2022;20(1):1972-1983**

Introduction

The electrochemical supercapacitor(Burke, 2000; Muthulakshmi, Kalpana, Pitchumani, & Renganathan, 2006; Sarangapani, Tilak, & Chen, 1996) is a charge storage device that can withstand more power than a battery and supply more energy than a traditional or electrolytic capacitor. There are three types of conducting polymer-based supercapacitors(Rudge, Davey, Raistrick, Gottesfeld, & Ferraris, 1994). Type one is a symmetric system in which the capacitor's electrodes are made of the same p-dupable conducting polymers. Type two is an asymmetric system that employs two p-dupable conducting polymers as electrode materials. Type three is a symmetric system depend on a conductive polymer that could utilized with both p- and n-doped electrodes. The electrochemical capacitor (EC), also known as a supercapacitor, is now widely accepted as one of the finest candidates for providing high power and long cycle life, which is critical for novel energy applications likewise hybrid electric vehicles, backup sources for numerous electrical devices, and uninterrupted power supplies (Afzal et al., 2017). As a result, researchers working in the field of energy storage devices must explore novel electrode materials for supercapacitors in order to meet the demands of high-power density and long durability devices. Electrochemical capacitors are classified as electrochemical double layer capacitors (EDLC) or pseudo capacitors based on the charge storage technique.

Correspondingauthor: Omar A. Hussein
Address: [1*]Department of Physics, College of Science, University of Diyala, Diyala, Iraq.
[2]Department of Physics, College of Science, University of Diyala, Diyala, Iraq.
[3]Department of Physics, College of Science, University of Baghdad, Baghdad, Iraq.

The charge separation at the electrode–electrolyte interface causes capacitance in the EDLC, while pseudo capacitance is caused by quick, reversible faradic redox processes on or near the electrode surface. Electronically conductive polymers (ECPs) have a feature over active carbon as a supercapacitor electrode material because they have both electrochemical double layer capacitance and pseudo capacitance, owing to the fast and reversible oxidation and reduction processes associated with the π-conjugated polymer chain (B. Kim, Ko, & Wallace, 2008; Woo, Dokko, & Kanamura, 2008). Polypyrene (PPy) polymer, an important conductive polymer, has been effectively used as a redox electrode material among numerous conductive polymers (Fan & Maier, 2006; Ko, Rhee, Park, & Kim, 1990; Rudge, Raistrick, Gottesfeld, & Ferraris, 1994). PPy and other conducting polymers, despite their excellent charge storage capacities, lack long-term stability and mechanical qualities (Abu-Saude & Morshed, 2018). To address this issue, a nanocomposite made up of PPy-NFs and inorganic transition metal oxide nanoparticles acting as ornament on polypyrene nanofibers has been proposed as the electrode material for a supercapacitor, with the synergistic impact of nanocomposite formation playing a key role in increasing the capacitance value. Furthermore, due to their large capacitance and fast redox kinetics, transition metal oxides have been suggested to be appropriate as electrode materials for pseudo capacitors (Cottineau, Toupin, Delahaye, Brousse, & Bélanger, 2006).

Recently, pseudo capacitance has been found in crystalline ferrites, particularly MnFe2O4 and CoFe2O4 (Kuo, Wu, & Letters, 2005). To the best of our knowledge, Co0.2Zn0.6Mn0.2Fe2O4 has not yet been investigated as a possibility for pseudo capacitor among other metal ferrites. As a result, it is worthwhile to examine the applicability of nanocomposites including PPy-NFs and nanocrystalline Co0.2Zn0.6Mn0.2Fe2O4 as electrode materials with high capacitance values in the field of demanding next generation miniaturized supercapacitors. Furthermore, because it is a economy and safe material, nanocrystalline Co0.6Zn0.2Mn0.2Fe2O4 could be a favorable candidate for supercapacitor.

Experimentalwork

Synthesis of Co0.6Zn0.2Mn0.2Fe2O4 nanoparticles

Synthesis of ferrite nanoparticles (Co0.2Zn0.6Mn0.2Fe2O4) was performed by the co-precipitation technology. This method is summarized as the following steps; we dissolve a stoichiometric amount of FeCl3 (8.1105g, 50 mM), MnCl2.4H2O (0.9895g, 5 mM) (AlPHA chemical), CoCl2 (2.5968g, 20 mM) (AlPHA chemical) and ZnCl2 (2.7257g, 20 mM) (ROMIL pure chemistry) in deionized water in independent beakers (see table 2). Then, they have been moved to another heat-resistant beaker with unbroken stirring to gain a uniform solution. As, in 100ml deionized water, sodium hydroxide (NaOH, 1.25 M L-1) (ROMIL pure chemistry) was dissolved separately. Then it was dropped in metal salt solution at 27°C until the pH reached 12, to make sure that metal ions are precipitated. After 60 min of heating at 90°C with constant stirring, the solution was turned off and permitted to cool at 27°C.The magnetic decantation process was used to separate and collect ferrite nanoparticles. Then, it had washed withdeionized water for several times by using a multi-funnels system. In NaOH solution (pH of 12), the moisture outcome has re-dispersed by stirring for 60 minutes. The heat treatment, which was done using the hydrothermal method, was the following step in the fabrication process. The colloidal solution was transferred to a 250 ml Teflon-lined autoclave reactor. After closing the autoclave tightly, it was positioned in a furnace at 250°C for 5 h. after a while, it let cool outdoor naturally at 27 0C. Then, the colloidal solution is filtered and washed with ethanol and deionized water several times for each one until PH even to 7. The material precipitate is ultimately place in the oven at 70 °C for 60 min to gain a stable phase of ferrite nanomaterial.

Synthesis of PPy nanofibers (PPy-NFs)

Throughout the technique, 2.5 mM (0.08185 g) methyl orange (MO) (LTD Rubilabor Chemical Co. Spain) was dissolved in de-ionized water (288 ml) and mixed with (14 mM) pyrrole monomer (Sigma Aldrich, China) to create a (Pyrrole monomer- methyl orange) solution, which was then iced to 30C through the use of an ice bath. For 10 minutes, the mixture was dynamically agitated until all agglomerates had vanished. In 33 ml de-ionized water, 1.702 (10mM) (FeCl3) (AlPHAchemica) is dissolved. Then, over the course of two hours, drop by drop into the (Py-MO) solution. In ice baths, these reaction solutions were

agitated for one day (24 hours). To separate the remaining contaminants (impurities) in PPy-NFs, the precipitated PPy-NFs were filtered and rinsed three times with acetone, alcohol, and water. Finally, the product was dried in an oven for six hours at 75 ° C.

PPy-NFs/ Co0.2Zn0.6Mn0.2Fe2O4 preparation

(3×10-2 g) of ferrite nanoparticles powder was dissolved in thirty milliliters of deionized water and sonicated for ten hours, whereas (3×10-2 g) of NFs-PPy was dissolved in thirty milliliters of distilled water and sonicated for two hours. Then, in volumetric ratio, Co0.2Zn0.6Mn0.2Fe2O4 solutions were added to the PPy-NFs solution. To fulfill a homogenous dispersion, the resultant solution was sonicated for 10 hours.

capacitor device Preparation

A nickel foam substance with dimensions of 1×1 cm2 was used to manufacture the supercapacitors electrodes from research materials. PPy-NFs, ferrite nanoparticles, and PPy-NFs nanocomposite were deposited on it using the drop casting method, and 1 ml of sulphuric acid (H2SO4) was added to evaluate its capacity using cyclic voltammetry (CV) curves, galvanostatic charge-discharge (GCD)measurements,and electrochemical impedance spectroscopy (EIS).

Results and Discussion

X-ray diffraction measurements

X-ray diffractometer had used to study the crystal structure to characterize the phase content of PPy-NFs and ferrite nanoparticles samples.

The XRD patterns of PPy-NFs are shown in Figure 1. The PPy-NFs powder is amorphous in form, meaning it is a non-crystalline solid with atom distribution that does not follow any crystalline structure, according to X-ray diffraction tests. The wide peak was caused by X-rays diffusing from the PPy-NFs chain. A broad peak can be seen in Fig. 1 at roughly 2 = 24.5°, which is assigned to the (102) directions (Hussein, Mubarak, & Ibrahim).

Amorphous PPy is distinguished for its broad peak. A broad halo pattern in the ranges 2 = 10 - 35 is attributed to PPy-NFs formed by oxidative polymerization and is typical of polypyrrole doped structures (MA, SG, PR, Shashwati, & VB, 2011; Ong, Ray, Cooney, Edmonds, & Easteal, 2008). According to the equation (1) that calculated the average chain separation (S) which calculates to be 4.53Å for polypyrrole nanofibers.

$$S=5\lambda/8\sin\theta \quad (1)$$

Here, λ and θ stands for the X-ray wavelengths and the diffraction angles at peaks of the amorphous Halo (Cheah, Forsyth, & Truong, 1998; Ouyang & Li, 1997) respectively.

As for the compound (Co0.2Zn0.6Mn0.2Fe2O4) in Figure 2, The X-ray diffractometer had recorded for 2θ values ranging 10-80 degrees. A cell parameteris examined for XRD analysis where the major peaks are (111), (220), (311), (222), (400), (422), (511), (440) and (533) matching with (Bhandare et al., 2020). They had indexed well in comparison with JCPDS # (74-2402), ICSD (01-074-2399) and Mn3O4 card No. (024-0734). The ferrite sample reveal usual cubic spinel peaks (Space group: Fd3m) and a single-phase structure for (Co0.2Zn0.6Mn0.2Fe2O4). As well it can conclude that Co2+, Zn2+ and Mn2+ ions are replaced in the ferrite construction. However, the analysis of phase assured the existence of Mn3O4 in the structure and the width of peaks confirms nanosize particles.

The experimental lattice parameter (aexp) had assessed using the formula below:

$$\mathbf{a_{exp} = d\sqrt{h^2 + k^2 + l^2}} \quad (2)$$

Where d represents the interplanar distance for each plane and (hkl) refer to Miller indices. The average crystallite size Dave had calculated by the following well-known Scherrer equation:

$$\mathbf{D_{ave} = K\lambda/\beta \cos\theta} \quad (3)$$

Where Dave denotes the average crystallite size, while K indicates to the Scherrer constant (K =0.94), λ is the wavelength of X-ray used, β refers to the full width at half maximum and θ is the Bragg angle. The cubic structure of the unit cell volume via equation (4) and The X-ray density dx were calculated from XRD data by using equation (5).

$$\mathbf{V_c = a_{exp}^3} \quad (4)$$

$$\mathbf{d_x = \frac{Z\,M}{N_A V_c}} \quad (5)$$

As Z represents the number of formula units in a unit cell (Z = 8 for spinel system), M is the molecular weight of the sample, NA is the Avogadro number and

Vc refers to the volume of the cell (Syue, Wei, Chou, &Fu, 2011).

The hopping lengths *LA*-A, *LB*-B and *LA*-B between the magnetic ions at the *A*-site and *B*-sites were estimated by the relations (Naseri & Saion, 2012):

$$\mathbf{L_{A-A}} = (\mathbf{a_{exp}}\sqrt{\mathbf{3}})/4 \quad (6)$$

$$\mathbf{L_{B-B}} = (\mathbf{a_{exp}}\sqrt{\mathbf{2}})/4 \quad (7)$$

$$\mathbf{L_{A-B}} = (\mathbf{a_{exp}}\sqrt{\mathbf{11}})/8 \quad (8)$$

Where *LA*-A, *LB*-B and *LA*-B are distances Tetra-tetra A-A, Octa-octa B-B, and Tetra-octa A-B, respectively.

Lattice constant (Å), average crystallite size, X-ray density, bonds lengths (Å), oxygen parameters, and hopping lengths for Zn0.8Mn0.2Fe2O4 ferrite are presented in Table1.

Table 1: XRD parameters of Co0.2Zn0.6Mn0.2Fe2O4 nanoparticles.

Sample	Lattice constant (Å)	Density of X-ray	Molecular mass	size crystallite	Hopping length (Å)		
	a_{exp}	$d_{x(\frac{g}{cm^3})}$	g/mol	D_{311}(nm)	L_{A-A}	L_{B-B}	L_{A-B}
$Co_{0.2}Zn_{0.6}Mn_{0.2}Fe_2O_4$	8.39	5.345	237.69	11.87	3.632	2.966	3.478

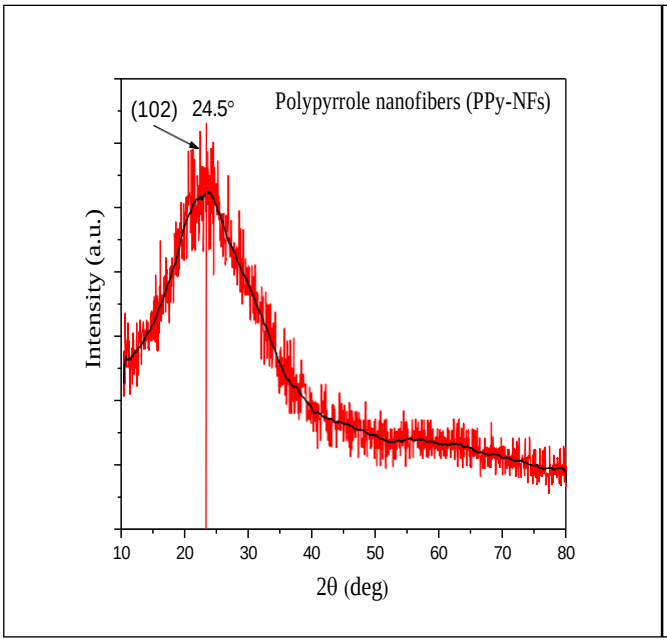

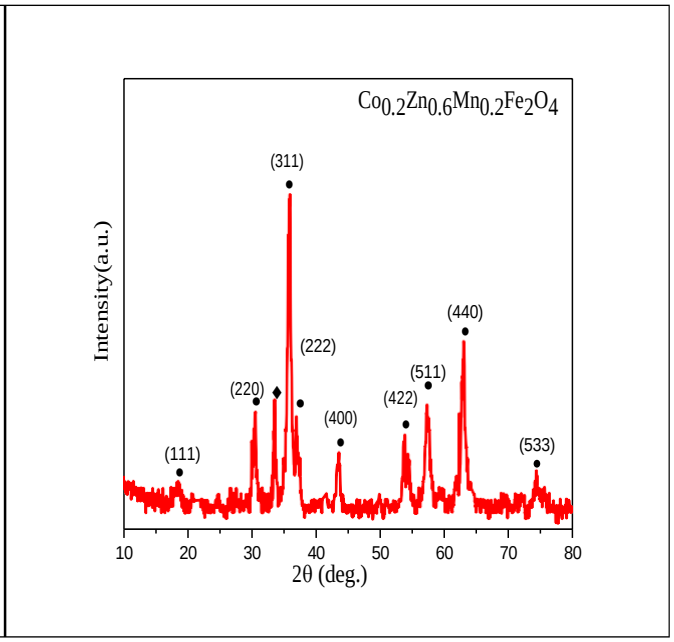

Figure 1: XRD pattern of (PPy-NFs).Figure 2: XRD result of Co0.2Zn0.6Mn0.2Fe2O4nanoparticles.

FESEM image analysis

The topographical and morphological features of composites and pure materials are revealed via FE-SEM. Figure 3 shows FESEM images of (PPy-NFs) samples generated utilizing the oxidative polymerization technique. All of the samples contain (1-D) nanofibers, which have a rough surface and come in a variety of dimensions, ranging from tens of microns in length to (50 to 130) nm in diameter. The micrograph clearly demonstrates a typical FESEM image of doped PPy-NFs, as well as the fact that nanostructures are made up of a network of densely entangled, coarse nanofibers.

Figure 4 shows a FESEM scan of ferrite nanoparticles with a densed view of the powder sample and relatively homogenous grain distribution. In addition, the magnetic particles were closely packed and arranged in a harmonic pattern. These micrographs reveal almost spherical particles with sizes ranging from 20 to 30 nanometers. As a result, the surface morphological and microstructure images match the XRD data quite well. In the samples, pores were discovered among the particles. The magnetic nanoparticles tended to clump (agglomeration) together because of their magnetic properties. Furthermore, developing forces such as capillary, electrostatic, and Van-der-Wall forces generate mutual interactions between nanoparticles, causing agglomeration.

The decoration of Polypyrrole nanofibers by ferrite nanoparticles to form PPy-NFs nanocomposite sample (PPy-NFs/Co0.2Zn0.6Mn0.2Fe2O4) had fabricated like a grainy surface structure. It had detected by FESEM. The FE-SEM images in Figure 5 indicate that the samples had ferrite nanoparticles stacked on the surface of the PPy-nanofibers. As a result, Figure 5 shows a progressive increase in ferrite on polymer fibers and an improvement in ferrite nanoparticle attachment. On the conductive polymer matrix, the magnetic particles are uniformly distributed. The composites have successfully mixed and merged homogeneously, as seen by this. Histograms represent diameters distribution of PPy-NFs and Co0.2Zn0.6Mn0.2Fe2O4nanoparticles that calculated by Image J software. It confirmed a well agreement with FE-SEM test that shown in Fig. 6.

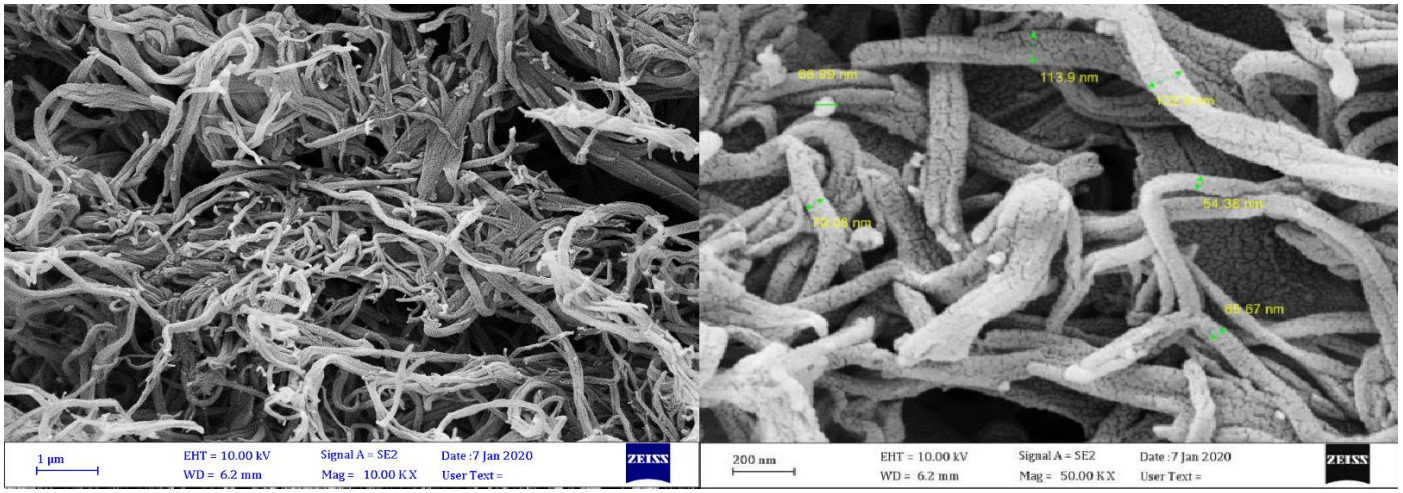

Figure 3: Different magnifications of FESEM images for polypyrrole nanofibers (PPy-NFs).

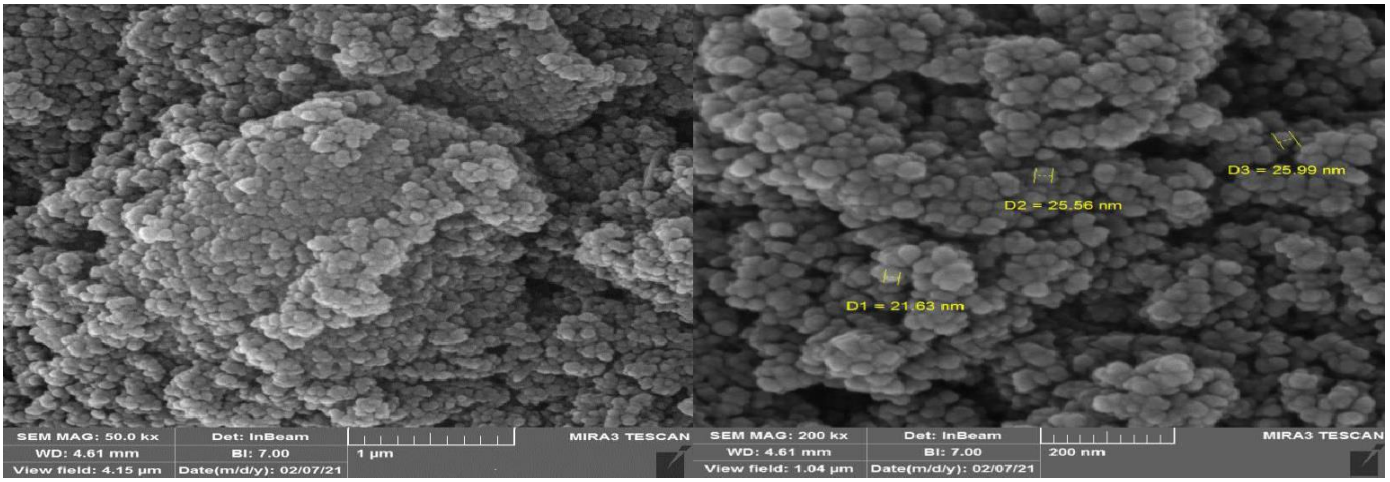

Figure 4: FESEM images of Co0.2Zn0.6Mn0.2Fe2O4 nanoparticles at different magnification.

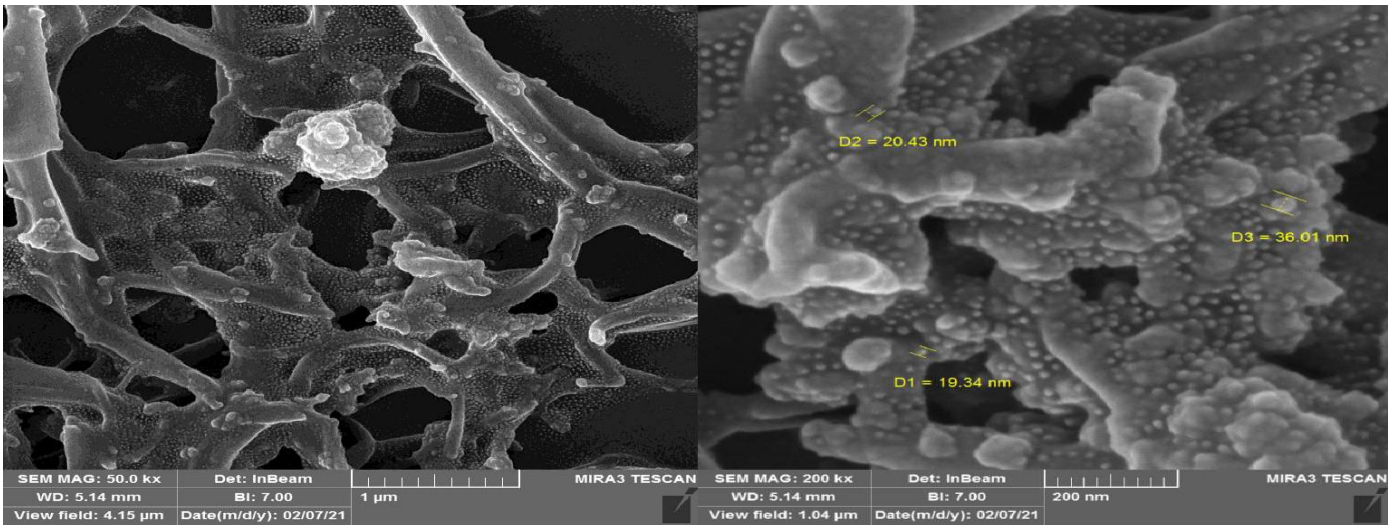

Figure 5: FESEM images of (PPy-NFs/Co0.2Zn0.6Mn0.2Fe2O4) nanocomposite at different magnification.

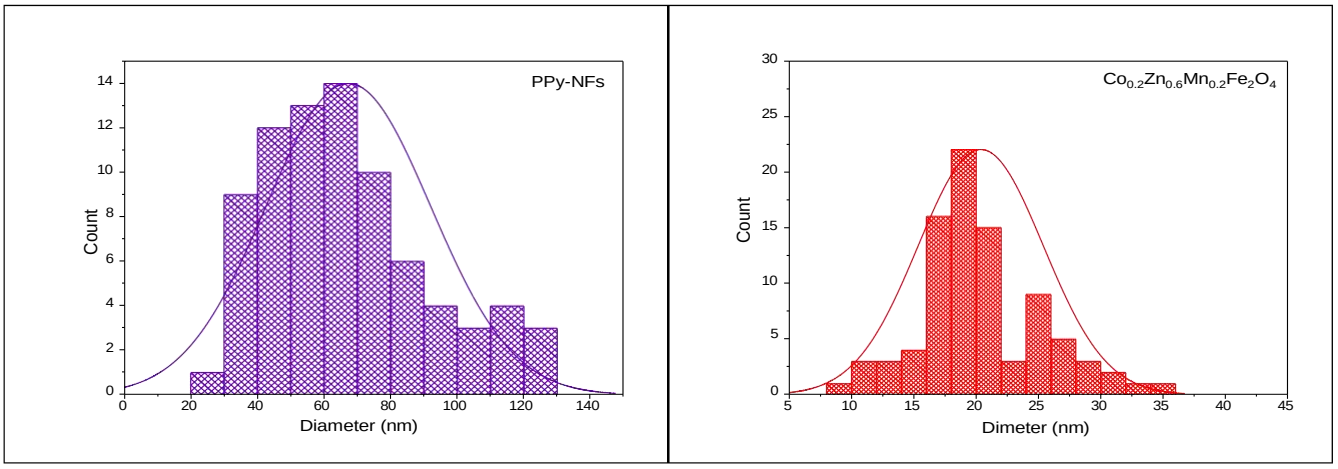

Figure 6: Histograms showing the diameter distribution of PPy-NFs and Co0.2Zn0.6Mn0.2Fe2O4nanoparticles.

Measurements of Electrochemical

Measurements of Cyclic voltammetry

The electrochemical features of the PPy-NFs, ferrite nanoparticles and PPy-NFs nanocomposites had described in the H2SO4 electrolyte. Electrochemical performance of samples had studied by cyclic voltammetry (CV), galvanostatic charge-discharge (GCD), and electrochemical impedance spectroscopy (EIS) measurements. Where, the influence of reinforcing PPy-NFs with certain ratio of ferrite nanoparticles on the (CV) and (GCD) curves and (EIS) outcomes had examined to gain the ideal electrochemical efficiency of electrodes. Thus, the PPy-NFs nanocomposite film combines the benefits of ferrite nanoparticles and polypyrrole nanofibers.

When evaluating the electrochemical behavior of a sample, all internal and external parameters should be taken into account. Because material features, cell

configurations, and experimental circumstances may vary, certain of these variables will have a direct impact on device performance. When it comes to CV measurements, particle size of active materials, electrolyte concentration, electrode thickness, scan rate, and working temperature all play an important role. (T. Kim et al., 2020) Electrochemical characteristics of metal oxides are also influenced by their crystal structure and cation distribution between tetrahedral (A) and octahedral (B) sites (Aparna, Grace, Sathyanarayanan, Sahu, & Compounds, 2018).

(CV) curves had utilized to usually describe of the electrochemical performance. Cyclic voltammetry (CV) curves of PPy-NFs, ferrite nanoparticles and PPy-NFs Nanocomposites in 1 ml sulphuric acid (H2SO4) at 20 mV/s scan rates. The impact of doping polypyrrole with numerous fractions of ferrite nanoparticles on (CV) outcomes had checked out in to gain the finest electrochemical efficiency of the PPy nanofibers electrode.

Ferrite nanoparticles (Zinc and Manganese ferrites) have important specific capacitances, necessitating further research. Conducting polymers like polypyrrole (PPy) and its derivatives, on the other hand, are interesting in supercapacitor electrode materials because of the enhanced pseudocapacitance potential they may produce (Liu et al., 2014). As a result, the advantages of ferrite nanoparticles and polypyrole nanofibers are combined to develop the electrochemical performance of the PPy-NFs/ferrite nanoparticles composite film.

Figure (7) shows the cyclic voltammetry for PPy-NFs samples with 20mv/s scan rate. Various potential window can be observed. For PPy-NFs, the potential widow is ranged from 1 to -1 V. Equation (9) can be used to calculate the specific capacitances (Cs) according to the value of the loop area which is represented by the corresponding figure for each CV curve and the value of the active mass for the electrode which is equal 0.2 mg/cm2. The specific capacitance of PPy-NFs is equal to 305 Fg-1, for the first cycle.

$$\mathbf{C} = \frac{\int \mathbf{IdV}}{\mathbf{2m\Delta V\, v}} (9)$$

Where C (Fg-1) denotes specific capacitance, I (A) refer the applied current, m (g) indicates for mass of active materials in electrode, v (mV/s) is scan rate and ΔV (V) refers to potential window in CV curves.

PPy-NFs sample shows anodic peak at less 0.9 V which may be results from the oxidative response of the PPy NFs electrode with the electrolyte, and cathodic peak position at -0.9V which results from the reductive response of the electrode with the electrolyte.

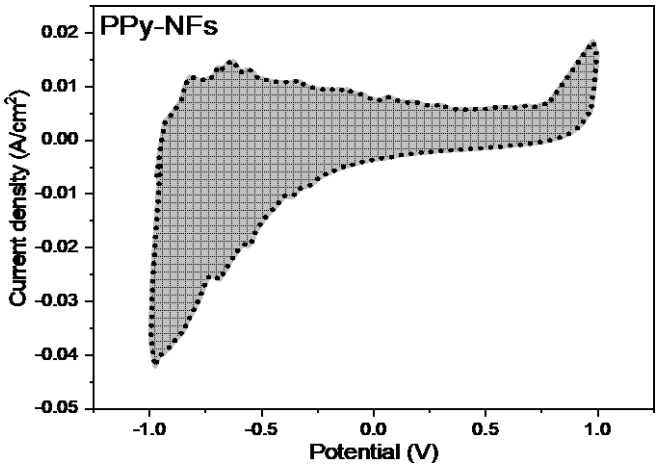

Figure 7: CV curves of the PPy-NFs.

Figure (8) shows the cyclic voltammetry for ferrite nanoparticles sample. According to above conditions (active mass, scan rate, potential widow and the area of the loop), the ferrite nanoparticles sample specific capacitance can be evaluated to equal 230.01 Fg-1.Through published researches about spinel metal ferrites, it was found that most of these materials are characterized by low cost of preparation, variable oxidation state, low resistance, large specific surface area and Excellent electrochemical activity.From figure (8), can say the periodic voltammograms of sample are roughly crescent in shape. Transition metal oxide for ferrite sample displays pseudo capacitive behavior through redox mechanism at the electrode surface. Where the electrochemical behavior in it arises from the presence of complex chemical composition and the synergistic impact of multiple valences of the metal cations. Also, Fe-based spinel mixed transition metal oxides reach redox reaction and improve electronic conductivity which is beneficial for electrochemical application.This agrees with researches on mixed transition metal oxides had examined as an electrode material for supercapacitor to enhance the energy density and overall performance. Where the storing of charge in it primarily originates from the pseudocapacitive mechanism (Raut & Sankapal, 2016). Ferrite electrode in basic electrolyte showed a redox hump (figure 8) which indicates a phenomenon to a degree of faradaic reactions.

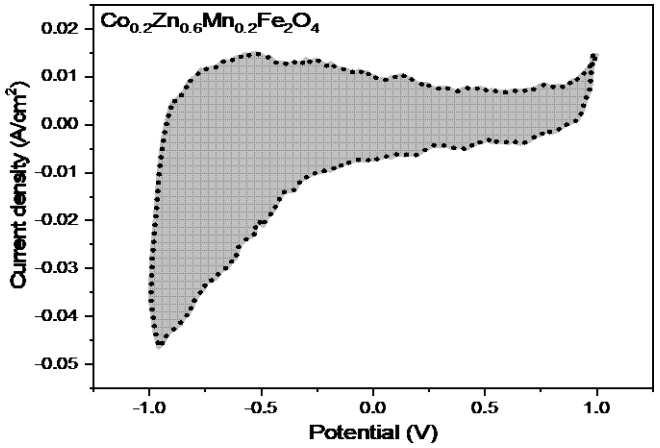

Figure 8: CV curves of the ferrite nanoparticles (Co0.2Zn0.6Mn0.2Fe2O4).

The current work was concentrated on new cost-effective method of PPy-NFs with spinel ferrite material to form PPy-NFs nanocomposite. The specific capacitances of PPy-NFs/Co0.2Zn0.6Mn0.2Fe2O4 are 370.39 Fg-1. The specific capacitance of PPy-NFs nanocomposite electrodes is bigger as compared to other one. Hence, it is confirmed that the PPy-NFs nanocomposite electrode reveals developed supercapacitive performance than PPy-NFs and ferrite electrode. This is because of the nanocomposite components have a greater synergistic effect. Where after addition of PPy-NFs and Because of its conductive nature, which results in more diffusion of ions into electroactive electrode material as well as harmony effect of components (Ishaq et al., 2019).

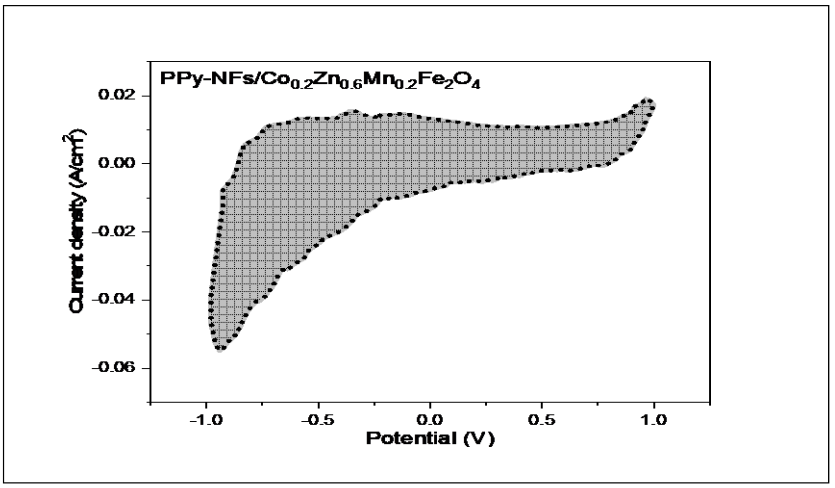

Figure 9: CV curves of the PPy-NFs nanocomposite (PPy-NFs/Co0.2Zn0.6Mn0.2Fe2O4) samples.

Electrochemical impedance spectroscopy investigation

The negative of the imaginary against the real parts of the complex impedance of electrochemical cells are shown by so-called Nyquist plots in electrochemical impedance spectroscopy (EIS). Figure (10) illustrates the plots of EIS spectra for the PPy nanofibers, ferrite nanoparticles and PPy-NFs nanocomposite cathodes with a frequency range of (0.1-200) kHz. EIS denotes a material resistance via which the material's conducting performance can be determined. In the high and low frequency ranges, the Nyquist plot contains semicircles and inclined straight lines, respectively. The charge transfer process at the electrode–electrolyte interface is represented by semicircles. As a result, a semicircle at high frequency intersecting at the x-axis (Z') denotes the equivalent series resistance (RESR), which includes the electrolyte's ionic resistance, the electrode material's electronic resistance, and the contact resistance at several phase interfaces. Though the charge transfer resistance (Rct) is represented by the semicircle in the high frequency range.

For the purpose of quantify the superior electrode, the Nyquist plots of the samples are shown in Figure (10). The measured values of RESR and Rct for the

synthesised samples are inserted in table (2). The Nyqust data reveals the truth of which the electrode has lower RESR and Rct than the others. It arranges things for finest charge transfer mechanisms. Hence small particles and larger surface area drives to better electrolyte penetration and electrolyte ion diffusion. Furthermore, the little frequency range for all samples shows an inclined plane at 450, which is connected to the material's pseudocapacitive characteristic (Shanmugavani & Selvan, 2014).

These results also confirm the excellent electrochemical cycle stability of the PPy-NFs, ferrite nanoparticles and PPy nanocomposites due to Synergistic effect of samples components which show potential application as electrode materials for electrochemical supercapacitors.

Table 2: RESR and Rct for the PPy-NFs, ferrite nanoparticles and PPy-NFs nanocomposites samples.

Sample code	Equivalent series resistance, R_{ESR} (Ω)	Charge transfer resistance, R_{ct} (Ω)
PPy-NFs	5.66	50.34
$Co_{0.2}Zn_{0.6}Mn_{0.2}Fe_2O$	7.13	30.49
PPy-NFs/$Co_{0.2}Zn_{0.6}Mn_{0.2}Fe_2O$	4.12	40.01

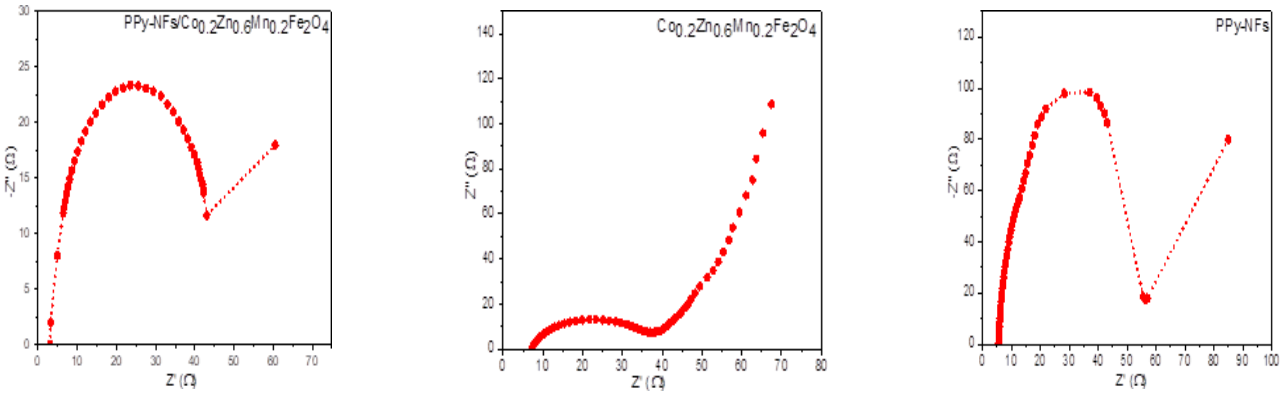

Figure 10: Nyquist plots for PPy-NFs, ferrite nanoparticles and PPy-NFs nanocomposite samples at (0.1 Hz- 200 KHz).

Galvanostatic charge-discharge measurements

To check electrochemical efficiency, a galvanostatic charge-discharge analysis has been used. The chargedischarge curves of the PPy-NFs, ferrite nanoparticles and PPy-NFs nanocompsites electrodes are shown in the figure (11). It has notices that, most of discharging curves of preparing electrode reveal imperfect straight lines. Thus, the Faradaic reaction occurs. Therefore, it exhibits supercapacitive feature. Internal resistance is highly significant and it is in charge of the initial potential drop. The internal resistance that based on the surface morphology of electrode and other factors attributes for the existence of interfacial contact resistance between 1M H2SO4 electrolyte and electrodes. For the active material loading, the interaction between ferrite nanoparticles and polypyrrole (PPy) in the polymer matrix are in charge for important alterations in the morphology of composite electrodes. Nevertheless, the resistance of supercapacitor is declined because of the creation of a large electrode/electrolyte contact surface area because of different morphologies of electrode. The discharging time of electrodes rises in the order of ferrite nanoparticles <PPy-NFs <PPy-NFs nanocomposites. This property might be due to the rise conductivity of synthesis electrodes that eases the fast charge transport in the

composite electrode (Scindia, Kamble, & Kher, 2019).

As can be seen from the above, the discharge time changes as the addition PPy-NFs vary. Furthermore, the CD curve of the PPy-NFs nanocomposite is less symmetrical than that of pure ferrite nanoparticles, indicating that the material's pesudocapacitance is enhanced by the addition of PPy-NFs. The synergistic impact of nanocomposite components is attributed to the increase in electrochemical performance of samples as shown by cyclic voltammetry and charge discharge studies.

GCD curves with lower current densities show increased faradic contribution (redox processes) to the charge accumulating process, and charge/discharge timings show superior electrochemical reversibility, indicating that these samples can be used in supercapacitors(Xu et al., 2015; Zhang et al., 2009).

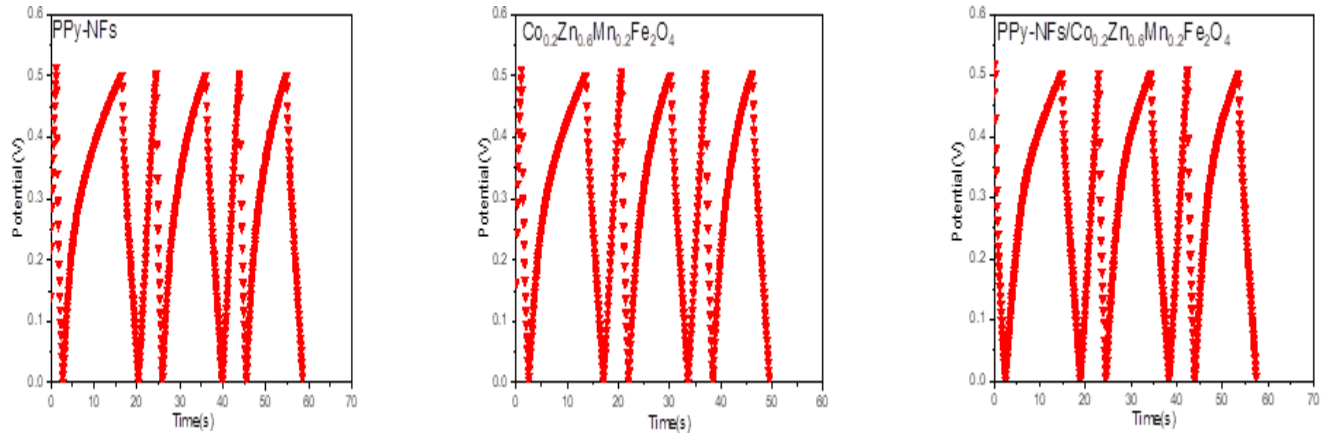

Figure 11: Galvanostatic charge-discharge for PPy-NFs, ferrite nanoparticles and PPy-NFs nanocomposite electrodes for supercapacitors.

Conclusions

Practical and modest techniques had used to manufacture PPy nanofibers (PPy-NFs), ferrite nanoparticles, and a PPy-NFs nanocomposite. These Materials have worked as electrodes in an electrochemical supercapacitor. The greatest capacitance value was (370.39 F/g) that stated by CV curves for PPy nanofibers that reinforced with ferrite nanoparticles. Even though the capacitance of PPy-NFs and ferrite are lower than PPy-NFs nanocomposite. As a result, doping plays a critical role in enhancing supercapacitor capacitance.

Reference

Abu-Saude, M., & Morshed, B. I. J. C. (2018). Characterization of a Novel Polypyrrole (PPy) conductive polymer coated patterned vertical CNT (pvCNT) Dry ECG electrode. 6(3), 27.

Afzal, A., Abuilaiwi, F. A., Habib, A., Awais, M., Waje, S. B., & Atieh, M. A. J. J. o. P. S. (2017). Polypyrrole/carbon

nanotube supercapacitors: Technological advances and challenges. 352, 174-186.
Aparna, M., Grace, A. N., Sathyanarayanan, P., Sahu, N. K. J. J. o. A., & Compounds. (2018). A comparative study on the supercapacitive behaviour of solvothermally prepared metal ferrite (MFe2O4, M= Fe, Co, Ni, Mn, Cu, Zn) nanoassemblies. 745, 385-395.
Bhandare, S. V., Kumar, R., Anupama, A., Choudhary, H., Jali, V., & Sahoo, B. J. C. I. (2020). Mechanistic insights into the sol-gel synthesis of complex (quaternary) Co–Mn–Zn-spinel ferrites: An annealing dependent study. 46(11), 17400-17415.
Burke, A. J. J. o. p. s. (2000). Ultracapacitors: why, how, and where is the technology. 91(1), 37-50.
Cheah, K., Forsyth, M., & Truong, V.-T. J. S. m. (1998). Ordering and stability in conducting polypyrrole. 94(2), 215-219.
Cottineau, T., Toupin, M., Delahaye, T., Brousse, T., & Bélanger, D. J. A. P. A. (2006). Nanostructured transition metal oxides for aqueous hybrid electrochemical supercapacitors. 82(4), 599-606.
Fan, L.-Z., & Maier, J. J. E. c. (2006). High-performance polypyrrole electrode materials for redox supercapacitors. 8(6), 937-940.
Hussein, O. A., Mubarak, T., & Ibrahim, I. M. Enhancement the photosensitivity of PPy-NFs/Nanoferrite for Photodetector.
Ishaq, S., Moussa, M., Kanwal, F., Ehsan, M., Saleem, M., Van, T. N., & Losic, D. J. S. r. (2019). Facile synthesis of ternary graphene nanocomposites with doped metal oxide and conductive polymers as electrode materials for high performance supercapacitors. 9(1), 1-11.
Kim, B., Ko, J., & Wallace, G. J. J. o. P. S. (2008). A novel capacitor material based on Nafion-doped polypyrrole. 177(2), 665-668.
Kim, T., Choi, W., Shin, H.-C., Choi, J.-Y., Kim, J. M., Park, M.-S., . . . Technology. (2020). Applications of voltammetry in lithium ion battery research. 11(1), 14-25.
Ko, J., Rhee, H., Park, S. M., & Kim, C. J. J. o. t. E. S. (1990). Morphology and electrochemical properties of polypyrrole films prepared in aqueous and nonaqueous solvents. 137(3), 905.
Kuo, S.-L., Wu, N.-L. J. E., & Letters, S.-S. (2005). Electrochemical capacitor of MnFe2O4 with NaCl electrolyte. 8(10), A495.
Liu, T., Finn, L., Yu, M., Wang, H., Zhai, T., Lu, X., . . . Li, Y. J. N. l. (2014). Polyaniline and polypyrrole pseudocapacitor electrodes with excellent cycling stability. 14(5), 2522-2527.
MA, C., SG, P., PR, G., Shashwati, S., & VB, P. J. S. n. l. (2011). Synthesis and characterization of polypyrrole (PPy) thin films. 2011.
Muthulakshmi, B., Kalpana, D., Pitchumani, S., & Renganathan, N. J. J. o. P. S. (2006). Electrochemical deposition of polypyrrole for symmetric supercapacitors. 158(2), 1533-1537.
Naseri, M. G., & Saion, E. B. J. A. i. c. p. (2012). Crystalization in spinel ferrite nanoparticles. 349-380.
Ong, C. K., Ray, S., Cooney, R. P., Edmonds, N. R., & Easteal, A. J. J. J. o. a. p. s. (2008). Preparation and characterization of composites of polyethylene with polypyrrole-coated wollastonite. 110(1), 632-640.
Ouyang, J., & Li, Y. J. P. (1997). Great improvement of polypyrrole films prepared electrochemically from aqueous solutions by adding nonaphenol polyethyleneoxy (10) ether. 38(15), 3997-3999.
Raut, S. S., & Sankapal, B. R. J. E. A. (2016). First report on synthesis of ZnFe2O4 thin film using successive ionic layer adsorption and reaction: approach towards solid-state symmetric supercapacitor device. 198, 203-211.
Rudge, A., Davey, J., Raistrick, I., Gottesfeld, S., & Ferraris, J. P. J. J. o. p. s. (1994). Conducting polymers as active materials in electrochemical capacitors. 47(1-2), 89-107.
Rudge, A., Raistrick, I., Gottesfeld, S., & Ferraris, J. P. J. E. A. (1994). A study of the electrochemical properties of conducting polymers for application in electrochemical capacitors. 39(2), 273-287.
Sarangapani, S., Tilak, B., & Chen, C. P. J. J. o. t. E. S. (1996). Materials for electrochemical capacitors: theoretical and experimental constraints. 143(11), 3791.
Scindia, S. S., Kamble, R. B., & Kher, J. A. J. A. A. (2019). Nickel ferrite/polypyrrole core-shell composite as an efficient electrode material for high-performance supercapacitor. 9(5), 055218.
Shanmugavani, A., & Selvan, R. K. J. R. A. (2014). Synthesis of ZnFe 2 O 4 nanoparticles and their asymmetric configuration with Ni (OH) 2 for a pseudocapacitor. 4(51), 27022-27029.
Syue, M.-R., Wei, F.-J., Chou, C.-S., & Fu, C.-M. J. T. S. F. (2011). Magnetic, dielectric, and complex impedance properties of nanocrystalline Mn–Zn ferrites prepared by novel combustion method. 519(23), 8303-8306.
Woo, S.-W., Dokko, K., & Kanamura, K. J. J. o. P. S. (2008). Composite electrode composed of bimodal porous carbon and polypyrrole for electrochemical capacitors. 185(2), 1589-1593.
Xu, R., Guo, F., Cui, X., Zhang, L., Wang, K., & Wei, J. J. J. o. M. C. A. (2015). High performance carbon nanotube based fiber-shaped supercapacitors using redox additives of polypyrrole and hydroquinone. 3(44), 22353-22360.
Zhang, Y., Feng, H., Wu, X., Wang, L., Zhang, A., Xia, T., . . . Zhang, L. J. I. j. o. h. e. (2009). Progress of electrochemical capacitor electrode materials: A review. 34(11), 4889-4899.